Functionalized Porous Nanoscale Fe$_3$O$_4$ Particles Supported Biochar From Peanut Shell For Pb(II) Ions Removal From Landscape Wastewater

Xiaojun Jin
Shaoxing University

Renrong Liu
Shaoxing University

Huifang Wang
Shaoxing University

Li Han
Shaoxing University

Muqing Qiu (✉ qiumuqing@usx.edu.cn)
Shaoxing University   https://orcid.org/0000-0002-2299-5374

Baowei Hu
Shaoxing University

Research Article

Abstract

The large amounts of heavy metal from landscape wastewater have become serious problems of environmental pollution and risks for human health. It affects the growth of plant and aquatic, and leads to the destruction of landscape. Therefore, the development of efficient novel adsorbent is a very important for treatment of heavy metal. A low-cost and easily obtained agricultural waste (Peanut Shell) was modified by nanoscale Fe_3O_4 particles. Then, the functionalized porous nanoscale Fe_3O_4 particles supported biochar from peanut shell (PS-Fe_3O_4) for removal of Pb(II) ions from aqueous solution was investigated. The characterization of PS-Fe_3O_4 composites showed that PS from peanut shell was successfully coated with porous nanoscale Fe_3O_4 particles. The pseudo second-order kinetic model and Langmuir model were more fitted for describing the adsorption process of Pb(II) ions in solution. The maximum adsorption capacity of Pb(II) ions removal in solution by PS-Fe_3O_4 composites could reach 188.68 mg/g. The adsorption process of Pb(II) ions removal by PS-Fe_3O_4 composites was a spontaneous and endothermic process. The adsorption mechanisms of Pb(II) ions by PS-Fe_3O_4 composites were mainly controlled by the chemical adsorption process. They included Fe-O coordination reaction, co-precipitation, complexation reaction and ion exchange. PS-Fe_3O_4 composites were thought as a low-cost, good regeneration performance and high efficiency adsorption material for removal of Pb(II) ions in solution.

1 Introduction

At present, the large amounts of heavy metal from landscape wastewater have become serious problems of environmental pollution and risks for human health. It affects the growth of aquatic, and leads to the destruction of landscape (Castaneda et al. 2019). In general, they mainly are discharged of untreated wastewater from metallurgical, mines, tanneries, textile, leather, etc. Many critical problems of heavy metal pollution on human health have been widely reported (Liu et al. 2010; Shi et al. 2019). Even at low concentration, these heavy metals in aquatic pollution would lead to occurrence of carcinogen in human according to US National Toxicology Program (Hokkanen et al. 2016). Therefore, it is a serious problem of aquatic pollution. It is necessary to search some desirable methods for solving above problems of heavy metal in aquatic pollution. Lead (Pb) is one of most hazardous, toxic and non-biodegradable heavy metals (Karunanayake et al. 2018). It can enter the human body through respiratory tract, food chain and drinking water (Thanh et al. 2018; Sahan 2019). Then, it accumulates in human body. Moreover, it would damage various organs and cause neurological dysfunction, anemia, kidney damage, and so on (Mouni et al. 2011; Ifthikar et al. 2017). According to report of World Health Organization (WHO) (Naushad et al. 2021), the concentration of Pb(II) ions in drinking water could not exceed about 10 µg/L. Therefore, some conventional separation technologies for Pb(II) removal are reported, such as ion-exchange, filtration membranes, electrolysis deposition, co-precipitation and coagulation processes (Cui et al. 2015; Huang et al. 2018). However, these separation technologies cannot be widely used in practical application because of expensive equipment, complex operation process, chemical pollution, and so on (Liang et al. 2021; Liu et al. 2021a). However, adsorption is recognized as an efficient technology for removal of pollutants. It is

high efficiency, low cost, environment-friendly, and simple operation (Chen et al. 2018). The development of efficient novel adsorbent is a very important for adsorption technology (Tang et al. 2018).

Biochar is a carbon-rich by-product from the pyrolysis of biomass, such as wood, crop straw, agricultural products, and so on. It was prepared at a certain temperature under hypoxia conditions (Qambrani et al. 2017; Qiu et al. 2021a). It has been regarded as a low-cost and environment-friendly multifunctional material for the removal of environmental pollutants, such as heavy metals, inorganic pollutants, organic pollutants, radionuclide, and so on (Hu et al. 2021; Lia et al. 2021; Liu et al. 2021b; Qiu et al. 2021b; Yao et al. 2021). Additionally, in order to improve the adsorption capacity of pollutants by biochar, varies methods were adopted to functionalize biochar. Xue et al. (2012) reported that Hydrogen peroxide modification enhances the ability of biochar produced from hydrothermal carbonization of peanut hull to remove aqueous heavy metals. The experimental results were desired. Ahmed et al. (2021) found that the adsorption capacity of Pb(II) ions in solution by the modified biochar from watermelon seeds were enhanced. The adsorption capacity reached 60.87 mg/g. However, they still had a shortcoming. That was, they were difficult to be separated them from aqueous solution after they adsorbed pollutants. The iron magnet-based materials could effectively solve this problem.

In recent years, magnetic Fe_3O_4 nanoparticle was applied extensively into the treatment of heavy metal in solution because of its characteristic of easy separation and high surface area (Shen et al. 2015). However, bare Fe_3O_4 nanoparticle was very easy to be oxidized and self-aggregated, which restricted its application for metal ion removal in aqueous solution (Alhokbany et al. 2019). Thus, surface protection and modification was a very important for the practical application of magnetic Fe_3O_4 nanoparticle (Xie et al. 2015). The combination of magnetic Fe_3O_4 nanoparticle with material as multiple composites was effective to improve its utility and stability. Pan et al. (2017) depicted that the Fe_3O_4 NPs was coated with organic acid could prevent the aggregation the Fe_3O_4 nanoparticle and enhance the adsorption capacity of the heavy metal in solution. Hou et al. (2021) reported that Novel SR-Fe_3O_4 material was fabricated by a facile method using mesoporous silica (RH-MCM-41). The maximum adsorption capacity of As(III) ions in solution by SR-Fe_3O_4 was 1002.03 mg/g. It was a good adsorbent material for removal of As(III) ions in aqueous solution. Therefore, it was very interesting to develop the nanoscale Fe_3O_4 particles supported biochar from biomass for heavy metals removal in solution. This could realize the 'win-win effect' between nanoscale Fe_3O_4 particles and biochar.

In this work, a low-cost and easily obtained agricultural waste (Peanut Shell) was modified by nanoscale Fe_3O_4 particles. Then, the functionalized porous nanoscale Fe_3O_4 particles supported biochar from peanut shell (PS-Fe_3O_4) for removal of Pb(II) ions from aqueous solution was investigated. Characteristics of biochar (PS) and PS-Fe_3O_4 composites were determined by SEM, TEM, EDS, FT-IR, XRD and XPS, respectively. The adsorption process and mechanism of Pb(II) removal in aqueous solution by PS-Fe_3O_4 composites would be explored in details. The experimental results of this research would provide a new idea for the ecological utilization of agricultural waste. The successful application of

peanut shells could not only effectively deal with heavy metal pollution, but also contribute to the recycling of peanut shells.

2 Experimental

2.1 Materials

Peanut shells were purchased from local market (Shaoxing, China). Milli-Q water (about 18MΩ/cm) was used in the experiments. Lead nitrate ($Pb(NO_3)_2$), iron chloride hexahydrate ($FeCl_3 \cdot 6H_2O$), ferrous sulfate heptahydrate ($FeSO_4 \cdot 7H_2O$), sulfuric acid (H_2SO_4), sodium hydroxide (NaOH) and hydrochloric acid (HCl) all were obtained from Shanghai McLean Biotechnology Co., Ltd. (Shanghai, China). All chemical reagents used were AR-grades without further purification.

2.2. Preparation of biochar and PS-Fe$_3$O$_4$ composites

For the preparation of biochar derived from peanut shell (PS), peanut shell sample was cleaned with Milli-Q water, and dried at 65 °C for 24 h. Then, the dried peanut shell sample was grounded, and sieved into 80 meshes. Next, 5.0 g of peanut shell sample was mixed with 20 mL of Milli-Q water, and continuously stirred at magnetic stirred for 20 min. The obtained mixture was placed into 50 mL of autoclave reactor, and heated at 150 °C for 24 h. Cooled at room temperature, and filtrated with qualitative filter paper. The obtained black precipitate was Milli-Q water for tree times, and dried at 105 °C for 24 h. The biochar derived from peanut shell was obtained.

For the preparation of the functionalized porous nanoscale Fe_3O_4 particles supported biochar from peanut shell (PS-Fe$_3$O$_4$), it was prepared according to the impregnation method (Maneechakr and Karnjanakom 2021). Briefly, 2.0 g of PS powder was added into 250 mL Erlenmeyer flask. Then, 25 mL of 0.2 mol/L Fe^{3+} and 25 mL of 0.1 mol/L Fe^{2+} were added, respectively. They were stirred for 10 min. Next, 50 mL of 0.5 mol/L NaOH solution was dropped into the mixture solution, and stirred for 20 min. Finally, PS-Fe$_3$O$_4$ composites were obtained with magnetic field, washed with Milli-Q water for three times, and dried at 105 °C for 24 h. The synthesis pathway for PS-Fe$_3$O$_4$ composites was depicted at Fig. 1.

2.3 Characterization

The samples of PS and PS-Fe$_3$O$_4$ were characterized by N_2-BET adsorption method, scanning electron microscope (SEM), energy dispersive X-ray spectra (EDS), transmission electron microscope (TEM), X-ray diffraction (XRD), Infrared spectrometer (FT-IR) and X-ray photoelectron spectroscopy (XPS), respectively. The details of those techniques were obtained in Supporting Information.

2.4 Adsorption experiments

To evaluate the adsorption process of Pb(II) ions in solution by PS-Fe$_3$O$_4$ composites, adsorption experiments were carried out under constant stirring. The details of adsorption experiments were provided in Supporting Information. Briefly, the certain amount of PS-Fe$_3$O$_4$ composites was added into a 250 mL

of Erlenmeyer flask. Then, 100 mL initial concentration of Pb(II) ions also was added into Erlenmeyer flask. Flask was sealed by bottle cap and placed in the shaker at 200 rpm and constant temperature. The pH in solution was adjusted with the 0.1 mol/L NaOH or 0.1 mol/L HCl solution. Concentration of Pb(II) ions in solution were analyzed by Flame Atomic Adsorption spectrophotometry, respectively (Fatehi et al. 2017). The residual sample was centrifuged at 4000 rpm for 20 min, and determined by microscopic technologies. All experiments were carried out for three times, and the experimental data were analyzed by the mean and standard deviation. Additionally, calculation equations of the uptake capacity (q(mg/g)) and the removal rate (R(%)) were provided in Supporting Information.

3 Results And Discussion

3.1 Characterization

The micro-morphologies of the PS and PS-Fe_3O_4 were characterized by the analytical technologies of SEM and TEM (Fig. 2). As shown from Fig. 2, the surface morphology of PS was smooth, and the surface morphology of PS-Fe_3O_4 was a craggy and irregular structure. It might be the reason that the PS-Fe_3O_4 composites were covered by porous nanoscale Fe_3O_4 particles. The EDS images also could confirm that porous nanoscale Fe_3O_4 particles were appeared and well distributed on the surface of PS (Fig. 3).
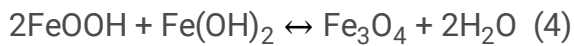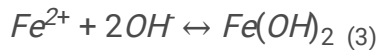
Figure 3a showed that C, O and Si elements were distributed in the structure of PS. Their contents were 68.47, 31.35 and 0.17%, respectively. It depicted that the elements of C and O were the main component in the material of PS. In addition to the appearance of C, O and Si elements, the element of Fe also was observed on the structure of PS-Fe_3O_4 composites (Fig. 3b). The content of Fe reached 20.67%. The contents of C, O and Si were 42.76, 36.29 and 0.25%, respectively. Compared with PS, the content of C was decreased, and the contents of O and Fe were increased. It could be confirmed that the functionalized porous nanoscale Fe_3O_4 particles supported by PS (PS-Fe_3O_4 composites) were successfully prepared.

The surface area and pore size of PS and PS-Fe_3O_4 composites were calculated by N_2 adsorption-desorption isotherms. Results showed that porous structure was present for PS-Fe_3O_4 composites. BET specific surface areas of PS and PS-Fe_3O_4 composites were 11.35 and 46.13 m^2/g, respectively. Due to nanoscale Fe_3O_4 particles supporting, the BET surface area of nanoscale was increased obviously compared with PS. It also depicted that PS could effectively decrease the aggregation of nanoscale Fe_3O_4 particles. The adsorption average pore width of nanoscale Fe_3O_4 particles were 6.94 and 6.31 nm, respectively. The results of FT-IR spectra about PS and PS-Fe_3O_4 composites were shown in Fig. 4a. The four strong characteristic peaks at 3398 cm^{-1}, 2330 cm^{-1}, 1610 cm^{-1} and 1377 cm^{-1} were observed. Some related researches indicated that the characteristic peak at 3398 cm^{-1} and 2330 cm^{-1} should be related to the stretching vibration of $-OH$ and $-C{\equiv}C$, respectively (Yuan et al. 2015). The stretching vibration peak at 1610 cm^{-1} contributed to the C=C, and the characteristic peak at 1377 cm^{-1} represented

the stretching vibration of C-O-C (Li et al. 2020). Compared with PS, the characteristic peak at 582 cm^{-1} was present on the surface of PS-Fe$_3$O$_4$ composites. The peak at 582 cm^{-1} corresponded to the stretching vibration of Fe-O. It also indicated that PS was coated with nanoscale Fe$_3$O$_4$ particles successfully. The crystal structures of PS and PS-Fe$_3$O$_4$ composites were determined by XRD patterns (Fig. 4b).

For PS, the peak at 26.58 º should be the characteristic peak of biochar. In addition to the peak at 26.58, the characteristic peak at 34.84 º also was observed on the surface of PS-Fe$_3$O$_4$ composites. According the related studies (Fatehi et al. 2017), it should be the appearance of Fe$_3$O$_4$ crystal structure on the surface of PS-Fe$_3$O$_4$ composites.

Formation of Fe$_3$O$_4$ particles could be depicted as following (Badi et al. 2018):

$$Fe^{3+} + 3OH^- \leftrightarrow Fe(OH)_3 \quad (1)$$
$$Fe(OH)_3 \leftrightarrow FeOOH + H_2O \quad (2)$$
$$Fe^{2+} + 2OH^- \leftrightarrow Fe(OH)_2 \quad (3)$$
$$2FeOOH + Fe(OH)_2 \leftrightarrow Fe_3O_4 + 2H_2O \quad (4)$$

According to the results of SEM, TEM, EDS, FT-IR, XRD and N$_2$-BET, it could be concluded that the functionalized porous nanoscale Fe$_3$O$_4$ particles supported PS from peanut shell was obtained. PS was successfully coated with the nanoscale PS-Fe$_3$O$_4$ particles. It was a craggy and irregular structure with BET specific surface area of 46.13 m^2/g and the adsorption average pore width of 6.31 nm.

3.2 Effect of operation parameters

The influence of operation parameters on the adsorption of Pb(II) ions in solution were very important for investigating the adsorption capacity of PS-Fe$_3$O$_4$ composites. In this research, the influences of contact time, initial concentration of Pb(II) ions in solution, initial pH in solution and temperature on the adsorption of Pb(II) ions in solution were tested. The details experiments could be found in Supporting Information. Effect of contact time on adsorption of Pb(II) ions in solution by PS-Fe$_3$O$_4$ composites was shown in Fig. 5a. The adsorption capacity of Pb(II) ions in solution by PS-Fe$_3$O$_4$ composites increased significantly with the increasing of contact time. At the first 100 min, the adsorption capacity of Pb(II) ions in solution increased rapidly. Then, it begun to increase slowly, and reached adsorption equilibrium. In the initial stage of adsorption process, there are a lot of adsorption sites on the surface of PS-Fe$_3$O$_4$ composites. They would facilitate adsorption process, and the adsorption capacity of Pb(II) ions in solution increased quickly. Then, as the contact time increased, the adsorption sites on the surface of PS-Fe$_3$O$_4$ composites begun to decrease. Therefore, the adsorption capacity of Pb(II) ions in solution increased slowly. The adsorption of Pb(II) ions in solution by PS-Fe$_3$O$_4$ composites reached adsorption equilibrium about 360 min.

Effect of initial concentration of Pb(II) ions in solution was depicted in Fig. 5b. Along with the increase of initial concentration of Pb(II) ions, the adsorption capacity of Pb(II) ions by PS-Fe_3O_4 composites increased. The high concentration gradient would accelerate the diffusion of Pb(II) ions to the PS-Fe_3O_4 composites (Song et al. 2016; Javaheri et al. 2019). The adsorption capacity of Pb(II) ions under different initial pH value conditions could be found in Fig. 5c. It could be seen that the adsorption capacity of Pb(II) ions in solution was increased with the increase of initial pH value at pH<6.0. It might be the reason that the large amount of H^+ ions at lower pH could generate electrostatic repulsion against Pb(II) ions. When the initial pH>6.0, the adsorption capacity of Pb(II) ions in solution begun to decrease. The increase of OH^- ions in solution could promote the precipitation formation of $Pb(OH)_2$ (Li et al. 2020). Effect of temperature on the adsorption capacity of Pb(II) ions in solution by PS-Fe_3O_4 composites was shown in Fig. 5d. It could be concluded that temperature was benefit for the adsorption capacity of Pb(II) ions in solution.

3.3 Adsorption kinetic, adsorption isotherm and thermodynamic

To evaluate the adsorption process of Pb(II) ions in solution by PS-Fe_3O_4 composites, adsorption kinetic, adsorption isotherm and thermodynamic were investigated according to the experimental data of Fig. 5. In this research, pseudo first-order kinetic model, pseudo second-order kinetic model, Langmuir isotherm model and Freundlich isotherm model were chosen for describing the adsorption process. The details of equations were provided in Supporting Information. The adsorption kinetics for adsorption of Pb(II) ions in solution by PS-Fe_3O_4 composites were described in Fig. 6a-b. It could be concluded that the pseudo second-order kinetic model was more fitted for describing the adsorption process of Pb(II) ions in solution (0.9989>0.9641). Therefore, it also could be confirmed that the adsorption process of Pb(II) ions in solution by PS-Fe_3O_4 composites was mainly controlled by the chemical adsorption process (Chen et al. 2019). Fig. 6c-d was the adsorption isotherms for adsorption of Pb(II) ions in solution by PS-Fe_3O_4 composites.

It could be observed that the R^2 of Langmuir model and Freundlich model were 0.9983 and 0.9374, respectively. Therefore, the adsorption process of Pb(II) ions in solution by PS-Fe_3O_4 composites could be depicted by the Langmuir model. It also could be implied that the adsorption processes were the homogeneous and monolayer adsorption (Zama et al. 2017). The maximum adsorption capacity of Pb(II) ions removal in solution by PS-Fe_3O_4 composites could reach 188.68 mg/g. Compared with the adsorption capacity of Pb(II) ions by other magnetic adsorbents, PS-Fe_3O_4 composites exhibited well performance of Pb(II) removal (The details of the adsorption capacity of Pb(II) ions in solution removal by other magnetic adsorbents could be found in Supporting Information). Therefore, PS-Fe_3O_4 composites were thought as a low-cost and high efficiency adsorption material for removal of Pb(II) ions in solution. According to the experimental data of Fig. 5d, thermodynamic parameters of Pb^{2+} ions in solution removal by PS-Fe_3O_4 composites could be calculated (They could be found in Supporting

Information). The negative value of ΔG^0 could be concluded that adsorption process of Pb(II) ions removal by PS-Fe$_3$O$_4$ composites was a spontaneous process. When reaction temperature increased, the value of ΔG^0 decreased. It indicated that temperature was benefit for enhancing adsorption capacity of Pb(II) ions removal by PS-Fe$_3$O$_4$ composites. Furthermore, ΔH^0 and ΔS^0 both were positive value. It also depicted that adsorption process of Pb(II) ions removal by PS-Fe$_3$O$_4$ composites also was an endothermic process.

3.4 Adsorption mechanism

In order to elaborate the adsorption mechanism of Pb(II) ions removal in solution by PS-Fe$_3$O$_4$ composites, the samples of PS-Fe$_3$O$_4$ composites before and after adsorption of Pb(II) ions also were characterized by XPS spectroscopy. The XPS spectra of PS-Fe$_3$O$_4$ composites before and after adsorption of Pb(II) ions were shown in Fig. 7.

As observed from Fig. 7a, the spectrum of C 1s, O 1s and Fe 2p at binding energies of 284.91, 530.69 and 710.52 eV appeared in the survey XPS spectrum before adsorption of Pb(II) ions. The elemental atomic compositions of C, O and Fe were 76.27, 20.28 and 3.45%, respectively. It was implied that the elements on the surface of PS-Fe$_3$O$_4$ composites were C, O and Fe. After adsorption of Pb(II) ions, the elemental atomic compositions of C, O and Fe on the surface of PS-Fe$_3$O$_4$ composites were changed. They were 64.69, 24.34 and 3.97%, respectively. Additionally, the new Pb 4f at binding energies of 143.26 eV appeared in the survey XPS spectrum. Therefore, it could be concluded that Pb(II) ions in solution could be successfully adsorbed by PS-Fe$_3$O$_4$ composites.

The spectrum of high resolved Pb 4f had two peaks at the binding energies of 138.41 and 143.41 eV (Fig. 7b). They were corresponded to Pb 4f$_{7/2}$ and Pb 4f$_{5/2}$, respectively. Additionally, they were in accordance with Pb(II) (Zhu et al. 2017). It also indicated that Pb(II) ions in solution should be adsorbed into the active sites on the surface of PS-Fe$_3$O$_4$ composites without being oxidized. This result was consistent with the result of the Fe 2p spectra (Fig. 7c). As from Fig. 7c, it could be observed that two characteristic peaks at the binding energies of 710.35 and 724.38 eV were presented on the surface of PS-Fe$_3$O$_4$ composites. They were corresponded to Fe(II) and Fe(III), respectively. The intensity of Fe 2p decreased after adsorption of Pb(II) ions in solution. It was indicated that PS-Fe$_3$O$_4$ composites could adsorb Pb(II) ions with Fe-O coordination reaction (Liu et al. 2016). Additionally, this result could also be confirmed from the O 1s spectra (Fig. 7d). The peak at binding energy of 531.35 eV was corresponded to Fe-O before adsorption of Pb(II) ions. After adsorption of Pb(II) ions, the intensity of O 1s increased. It was implied that the interaction of PS-Fe$_3$O$_4$ composites and Pb(II) ions was happened through Fe-O coordination reaction. According to the result of influence of initial pH, it could be concluded that pH had an important effect on the adsorption capacity of Pb(II) ions in solution. The initial pH in solution not only affected the charges of functional groups on the surface of PS-Fe$_3$O$_4$ composites, but also affected the species of Pb(II) ions in solution. Therefore, PS-Fe$_3$O$_4$ composites could adsorb the Pb(II) ions in solution through electrostatic interaction. Additionally, Pb(II) ions in solution could be co-precipitated on the

surface of PS-Fe_3O_4 composites. The related equations were following, such as, $Fe_3O_4 + 8H^+ \rightarrow Fe^{2+} + 2Fe^{3+} + 4H_2O$ and $Pb^{2+} + 2OH^- \rightarrow Pb(OH)_2\downarrow$. As shown from the results of FT-IR, the large number of functional groups (such as $-OH$, $-C\equiv C$, $C=C$, C-O-C and Fe-O functional groups) were appeared on the surface of PS-Fe_3O_4 composites. They could interact with Pb(II) ions in solution through complexation reaction, ion exchange and Fe-O coordination reaction.

In a word, the adsorption process of Pb(II) ions in solution by PS-Fe_3O_4 composites was mainly controlled by the chemical adsorption process. The possible reaction mechanisms of Pb(II) ions removal by PS-Fe_3O_4 composites were depicted in Fig. 8. The possible mechanism of Pb(II) ions by PS-Fe_3O_4 composites included Fe-O coordination reaction, co-precipitation, complexation reaction and ion exchange.

3.5 Regeneration experiment

In order to investigate the regeneration of Pb(II) ions removal by PS-Fe_3O_4 composites, the adsorption or desorption experiment of Pb(II) ions removal by PS-Fe_3O_4 composites were carried out. After the adsorption experiment of Pb(II) ions removal by PS-Fe_3O_4 composites reached equilibrium, the solution was centrifuged at 4000 rpm for 20 min and the adsorbent of PS-Fe_3O_4 composites was obtained. Next, they were washed for three times with 0.1 M H_2SO_4, and dried at 60℃ for 24 h. Then, the dried PS-Fe_3O_4 composites were used for adsorption experiment again. The experimental results were depicted in Fig. 9. After four regeneration experiments, the adsorption capacity of Pb(II) ions removal by PS-Fe_3O_4 composites only decreased slightly, and it still retained 71.86%. It also could be implied that PS-Fe_3O_4 composites were reused for Pb(II) ions in solution removal, the regeneration performance of PS-Fe_3O_4 composites was good.

4 Conclusions

The functionalized porous nanoscale Fe_3O_4 particles supported biochar from peanut shell (PS-Fe_3O_4) for removal of Pb(II) ions from aqueous solution was investigated. PS and PS-Fe_3O_4 composites were characterization by SEM, TEM, EDS, FT-IR, XRD and XPS, respectively. It was a craggy and irregular structure with BET specific surface area of 46.13 m^2/g and the adsorption average pore width of 6.31 nm. The large number of functional groups (such as $-OH$, $-C\equiv C$, $C=C$, C-O-C and Fe-O functional groups) were appeared on the surface of PS-Fe_3O_4 composites. The adsorption process of Pb(II) ions in solution by PS-Fe_3O_4 composites was mainly controlled by the chemical, homogeneous and monolayer, spontaneous and endothermic adsorption process. The adsorption mechanisms of Pb(II) ions by PS-Fe_3O_4 composites were Fe-O coordination reaction, co-precipitation, complexation reaction and ion exchange. PS-Fe_3O_4 composites were thought as a low-cost, good regeneration performance and high efficiency adsorption material for removal of Pb(II) ions in solution.

Declarations

Ethical Approval

This section is "not applicable" for this study.

Consent to Participate

Not applicable.

Consent to Publish

All authors reviewed and approved the manuscript for publication.

Authors Contributions

Huifang Huang and Renrong Liu designed the experiment, Li Han and Xiaojun Jin performed the experiment. Muqing Qiu processed the experimental data and wrote this article. Baowei Hu revised this paper.

Competing Interests

The authors declare no competing interests.

Availability of data and materials

The data and materials presented in this study are available on request from the corresponding author. The data are not publicly available due to privacy restrictions.

References

1. Ahmed W, Mehmood S, Núñez-Delgado A, Ali S, Qaswar M, Shakoor A, Mahmood M, Chen DY (2021) Enhanced adsorption of aqueous Pb(II) by modified biochar produced through pyrolysis of watermelon seeds. Sci Total Environ 784:147136
2. Alhokbany N, Ahamad T, Naushad M, Alshehri S (2019) Feasibility of toxic metal removal from aqueous medium using schiff-base based highly porous nanocomposite: adsorption characteristics and post characterization. J Mol Liq 294:111598

3. Badi MY, Azari A, Pasalari H, Esrafili A, Farzadkia M (2018) Modification of activated carbon with magnetic Fe_3O_4 nanoparticle composite for removal of ceftriaxone from aquatic solutions. J Mol Liq 261:146–154

4. Castaneda LF, Coreno O, Nava JL (2019) Arsenic and hydrated silica removal from groundwater by electrocoagulation using an up-flow reactor in a serpentine array. J Environ Chem Eng 7:103353

5. Chen J, Yu M, Wang C, Feng J, Yan W (2018) Insight into the synergistic effect on selective adsorption for heavy metal ions by apolypyrrole/TiO_2 composite. Langmuir 34:10187–10196

6. Chen Q, Zheng J, Yang Q, Dang Z, Zhang L (2019) Effect of carbon chain structure on the phthalic acid esters (PAEs) adsorption mechanism by mesoporous cellulose biochar. Chem Eng J 362:383–391

7. Cui J, Jing C, Che D, Zhang J, Duan S (2015) Groundwater arsenic removal by coagulation using ferric (III) sulfate and polyferric sulfate: a comparative and mechanistic study. J Environ Sci 32:42–53

8. Fatehi MH, Shayegan J, Zabihi M, Goodarznia I (2017) Functionalized magnetic nanoparticles supported on activated carbon for adsorption of Pb(II) and Cr(VI) ions from saline solutions. J Environ Chem Eng 5:1754–1762

9. Hou J, Weng R, Jiang W, Sun H, Xia J, Liu Y, Sheng J, Song Y (2021) In-situ preparation of novel sedimentary rock-like Fe_3O_4 by rice-husk mesoporous silica as templates for effective remove As(III) from aqueous solution. J Environ Chem Eng 9:105866

10. Hokkanen S, Bhatnagar A, Repo E, Lou S, Sillanpää M (2016) Calcium hydroxyapatite microfibrillated cellulose composite as a potential adsorbent for the removal of Cr (VI) from aqueous solution. Chem Eng J 283:445–452

11. Hu B, Wang H, Liu R, Qiu M (2021) Highly efficient U(VI) capture by amidoxime/carbon nitride composites: Evidence of EXAFS and modeling, Chemosphere, 274, 129743

12. Huang Y, Wu D, Wang X, Huang W, Lawless D, Feng X (2018) Removal of heavy metals from water using polyvinylamine by polymer-enhanced ultrafiltration and flocculation. Sep Purif Technol 158:124–136

13. Karunanayake AG, Todd OA, Crowley M, Ricchetti L, Pittman CU, Anderson R, Mohan D, Mlsna T (2018) Lead and cadmium remediation using magnetized and nonmagnetized biochar from Douglas fir. Chem Eng J 331:480–491

14. Javaheri F, Kheshti Z, Ghasemi S, Altaee A (2019) Enhancement of Cd^{2+} removal from aqueous solution by multifunctional mesoporous silica: equilibrium isotherms and kinetics study. Sep Purif Technol 224:199–208

15. Lia Q, Chen Z, Wang H, Yang H, Wen T, Wang S, Hu B, Wang X (2021) Removal of organic compounds by nanoscale zero-valent iron and its composites. Sci Total Environ 792:148546

16. Liang L, Xi F, Tan W, Meng X, Hu B, Wang X (2021) Review of organic pollutants and heavy metals removal by biochar and biochar-based composites. Biochar 3:255–281

17. Liu F, Hua S, Wang C, Qiu M, Jin L, Hu B (2021a) Adsorption and reduction of Cr(VI) from aqueous solution using cost-effective caffeic acid functionalized corn starch. Chemosphere 279:130539

18. Liu R, Wang H, Han L, Hu B, Qiu M (2021b) Reductive and adsorptive elimination of U(VI) ions in aqueous solution by SFeS@Biochar composites, Environ. Sci. Pollut. R., 2021, DOI:10.1007/s11356-021-14835-0

19. Liu T, Li S, Liu Y, Guo Q, Wang L, Liu D, Zhou J (2016) Magnetic polydopamine decorated with Mg-Al LDH nanoflakes as a novel bio-based adsorbent for simultaneous removal of potentially toxic metals and anionic dyes. J Mater Chem A 4:1737–1746

20. Li Y, Zhang X, Zhang P, Liu X, Han L (2020) Facile fabrication of magnetic bio-derived chars by co-mixing with Fe_3O_4 nanoparticles for effective Pb^{2+} adsorption: properties and mechanism. J Clean Prod 262:121350

21. Liu W, Zhang J, Zhang C, Wang Y, Li Y (2010) Adsorptive removal of Cr (VI) by Femodified activated carbon prepared from Trapanatans husk. Chem Eng J 162:677–684

22. Maneechakr P, Karnjanakom S (2021) Facile utilization of magnetic MnO_2@Fe_3O_4@sulfonated carbon sphere for selective removal of hazardous Pb(II) ion with an excellent capacity: Adsorption behavior/isotherm/kinetic/thermodynamic studies. J Environ Chem Eng 9:106191

23. Mouni L, Merabet D, Bouzaza A, Belkhiri L (2011) Adsorption of Pb(II) from aqueous solutions using activated carbon developed from Apricot stone. Desalination 276:148–153

24. Naushad M, Ahamad T, Al-sheetan K (2021) Development of a polymeric nanocomposite as a high performance adsorbent for Pb(II) removal from water medium: equilibrium, kinetic and antimicrobial activity. J Hazard Mater 407:124816

25. Ifthikar J, Wang J, Wang Q, Wang T, Wang H, Khan A, Jawad A, Sun T, Jiao X, Chen Z (2017) Highly efficient lead distribution by magnetic sewage sludge biochar: sorption mechanisms and bench applications. Bioresour Technol 238:399–406

26. Pan Z, Li W, Fortner JD, Giammar DE (2017) Measurement and surface complexation modeling of U(VI) adsorption to engineered iron oxide nanoparticles. Environ Sci Technol 51:9219–9226

27. Qiu M, Hu B, Chen Z, Yang H, Wang X (2021a) Challenges of organic pollutant photocatalysis by biochar-based catalysts. Biochar 3:117–123

28. Qiu M, Liu Z, Wang S, Hu B (2021b) The photocatalytic reduction of U(VI) into U(IV) by ZIF-8/g-C_3N_4 composites at visible light. Environ Res 196:110349

29. Qambrani NA, Rahman MM, Won S, Shim S, Ra C (2017) Biochar properties and eco-friendly applications for climate change mitigation, waste management, and wastewater treatment: a review. Renew Sustain Energy Rev 79:255–273

30. Sahan T (2019) Application of RSM for Pb(II) and Cu(II) adsorption by bentonite enriched with single bond -SH groups and a binary system study, J. Water Proc. Eng., 31, 100867

31. Shen P, Zhang H, Liu H, Xin J, Fei L, Luo X, Ma R, Zhang S (2015) Core-shell Fe_3O_4@SiO_2@$HNbMoO_6$ nanocomposites: new magnetically recyclable solid acid for heterogeneous catalysis. J Mater Chem

A 3:3456–3464

32. Shi Q, Terracciano A, Zhao Y, Wei C, Christodoulatos C, Meng X (2018) Evaluation of metal oxides and activated carbon for lead removal: kinetics, isotherms, column tests, and the role of co-existing ions. Sci Total Environ 648:176–183

33. Song X, Niu Y, Qiu Z, Zhang Z, Zhou Y, Zhao J, Chen H (2016) Adsorption of Hg(II) and Ag(I) from fuel ethanol by silica gel supported sulfur-containing pamam dendrimers: kinetics, equilibrium and thermodynamics. Fuel 206:80–88

34. Tang N, Niu C, Li X, Liang C, Guo H, Lin L, Zheng C, Zeng G (2018) Efficient removal of Cd(2+) and Pb(2+) from aqueous solution with amino- and thiol-functionalized activated carbon: Isotherm and kinetics modeling. Sci Total Environ 635:1331–1344

35. Thanh HT, Phuong TT, Hang PT, Toan TT, Tuyen TN, Mau TX, Khieu DQ (2018) Comparative study of Pb(II) adsorption onto MIL−101 and Fe−MIL−101 from aqueous solutions. J Environ Chem Eng 6:4093–4102

36. Xie M, Zeng L, Zhang Q, Kang Y, Xiao H, Peng Y, Chen X, Luo J (2015) Synthesis and adsorption behavior of magnetic microspheres based on chitosan/organic rectorite for low-concentration heavy metal removal. J Alloys Compd 647:892–905

37. Xue Y, Gao B, Yao Y, Inyang M, Zhang M, Zimmerman AR, Ro KS (2012) Hydrogen peroxide modification enhances the ability of biochar (hydrochar) produced from hydrothermal carbonization of peanut hull to remove aqueous heavy metals: Batch and column tests.Chem. Eng. J.,200–202, 673–680

38. Yao L, Yang H, Chen Z, Qiu M, Wang HuB X (2021) Bismuth oxychloride-based materials for the removal of organic pollutants in wastewater. Chemosphere 273:128576

39. Yuan H, Lu T, Huang H, Zhao D, Kobayashi N, Chen Y (2015) Influence of pyrolysis temperature on physical and chemical properties of biochar made from sewage sludge. J Anal Appl 112:284–289

40. Zama EF, Zhu Y, Reid BJ, Sun G (2017) The role of biochar properties in influencing the sorption and desorption of Pb(II), Cd(II) and As(III) in aqueous solution. J Clean Prod 148:127–136

41. Zhu M, Zhu L, Wang J, Yue T, Li R, Li Z (2017) Adsorption of Cd(II) and Pb(II) by in situ oxidized Fe_3O_4 membrane grafted on 316L porous stainless steel filter tube and its potential application for drinking water treatment. J Environ Manag 196:127–136
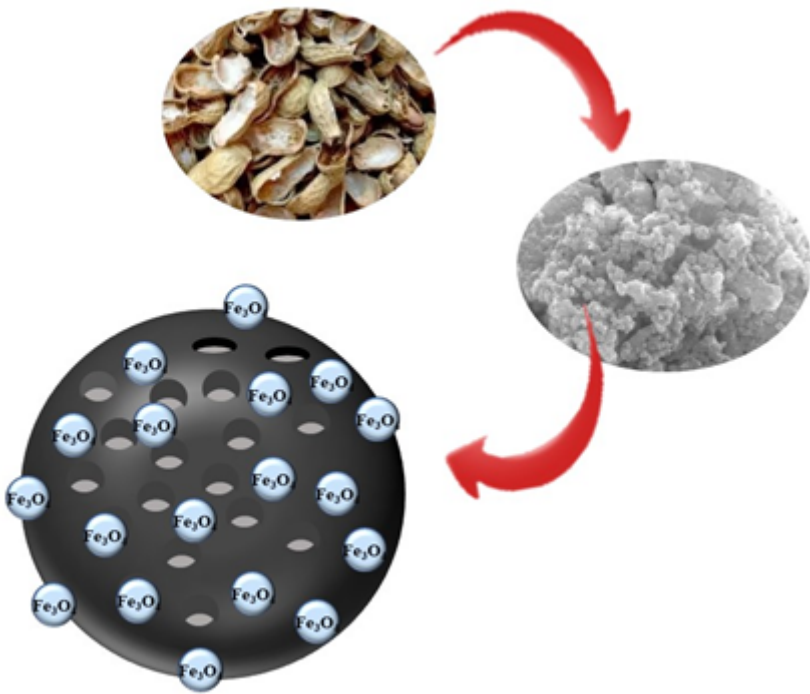
Figures

Figure 1
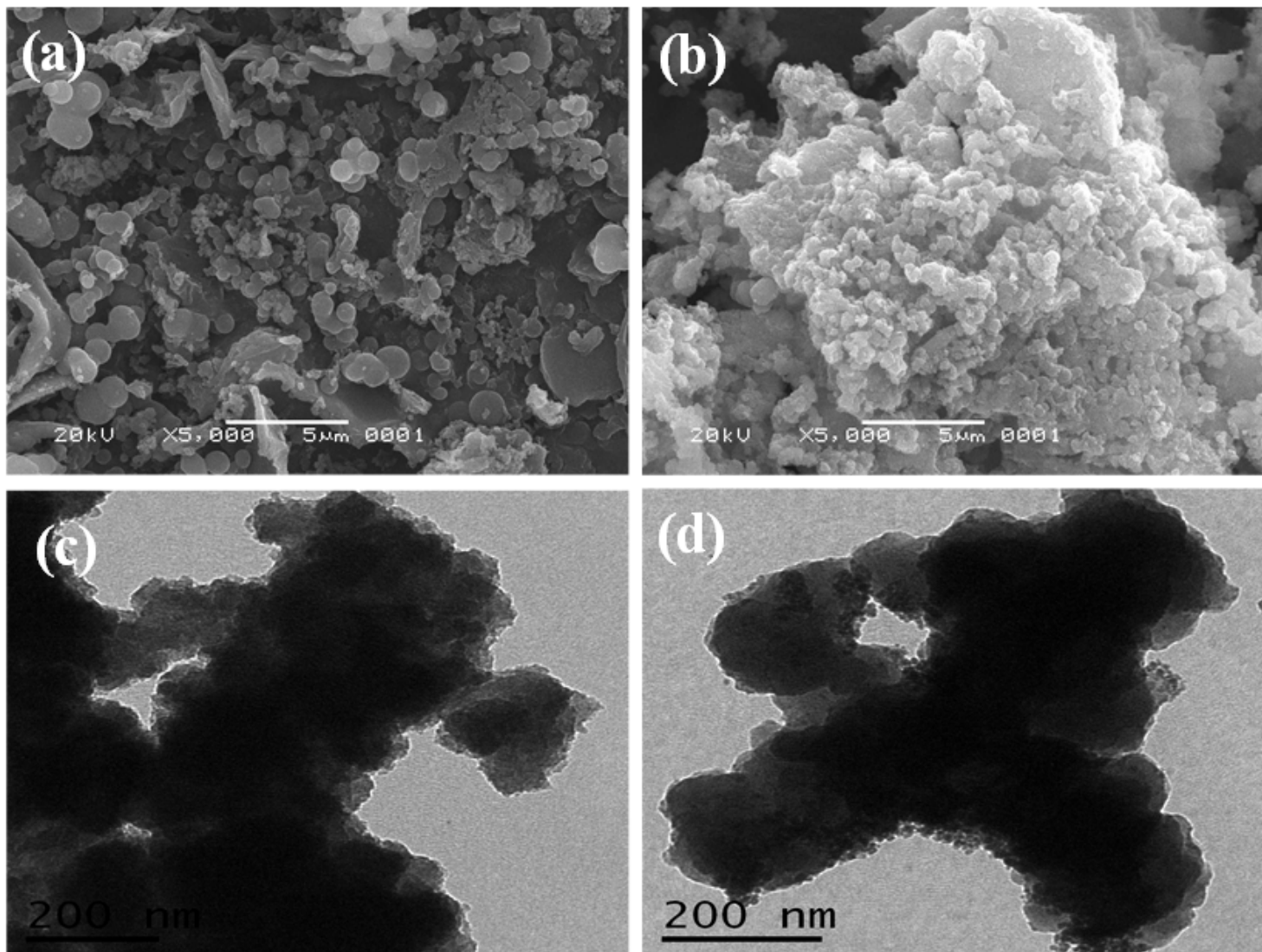
The synthesis pathway for PS-Fe3O4 composites

Figure 2

SEM images of PS (a) and PS-Fe3O4 (b); TEM images of PS (c) and PS-Fe3O4 (d)
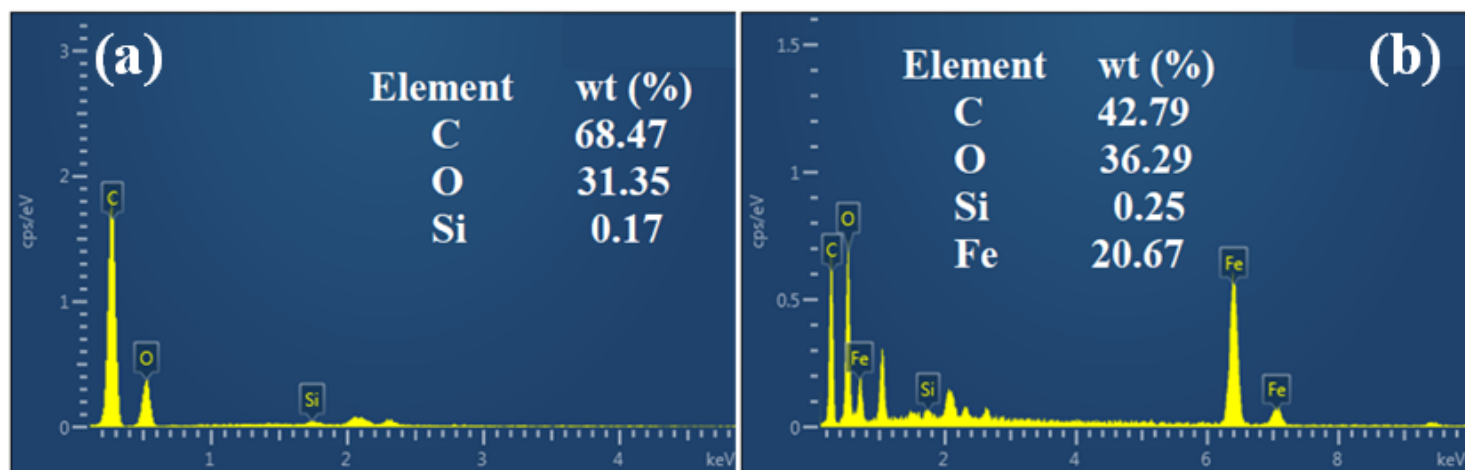

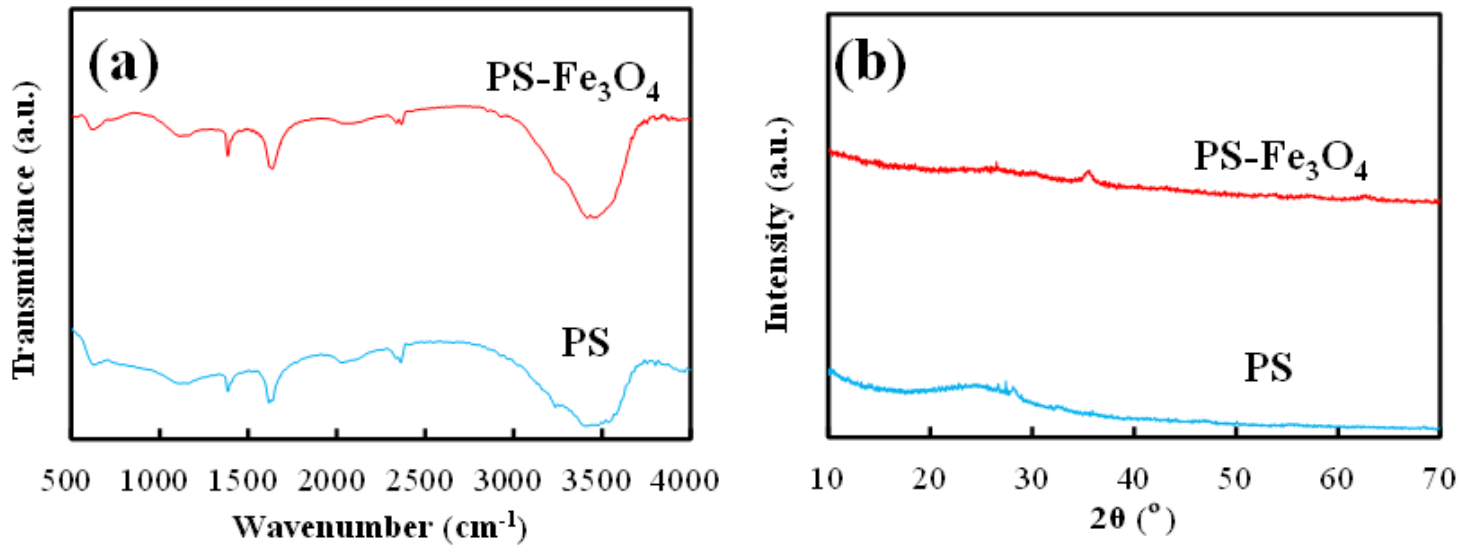**Figure 3**

EDS images of PS (a) and PS-Fe3O4 (b)

Figure 4

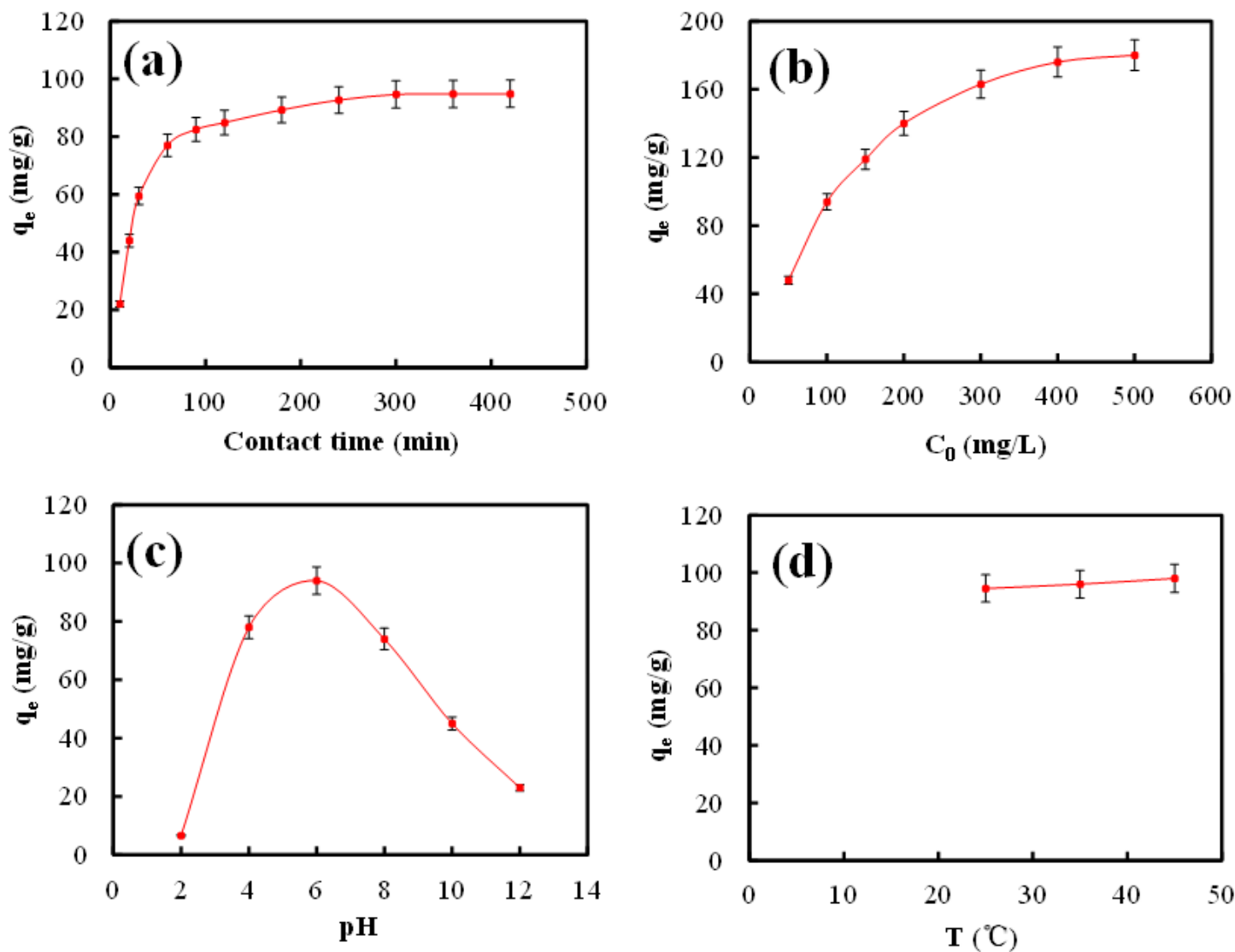FT-IR spectra of PS and PS-Fe3O4 (a) and XRD patterns of PS and PS-Fe3O4 (b)

Figure 5

Effect of operation parameters on the adsorption of Pb(II) ions in solution by PS-Fe3O4 composites (a: contact time, b: initial concentration of Pb(II) ions in solution, c: pH and d: temperature)
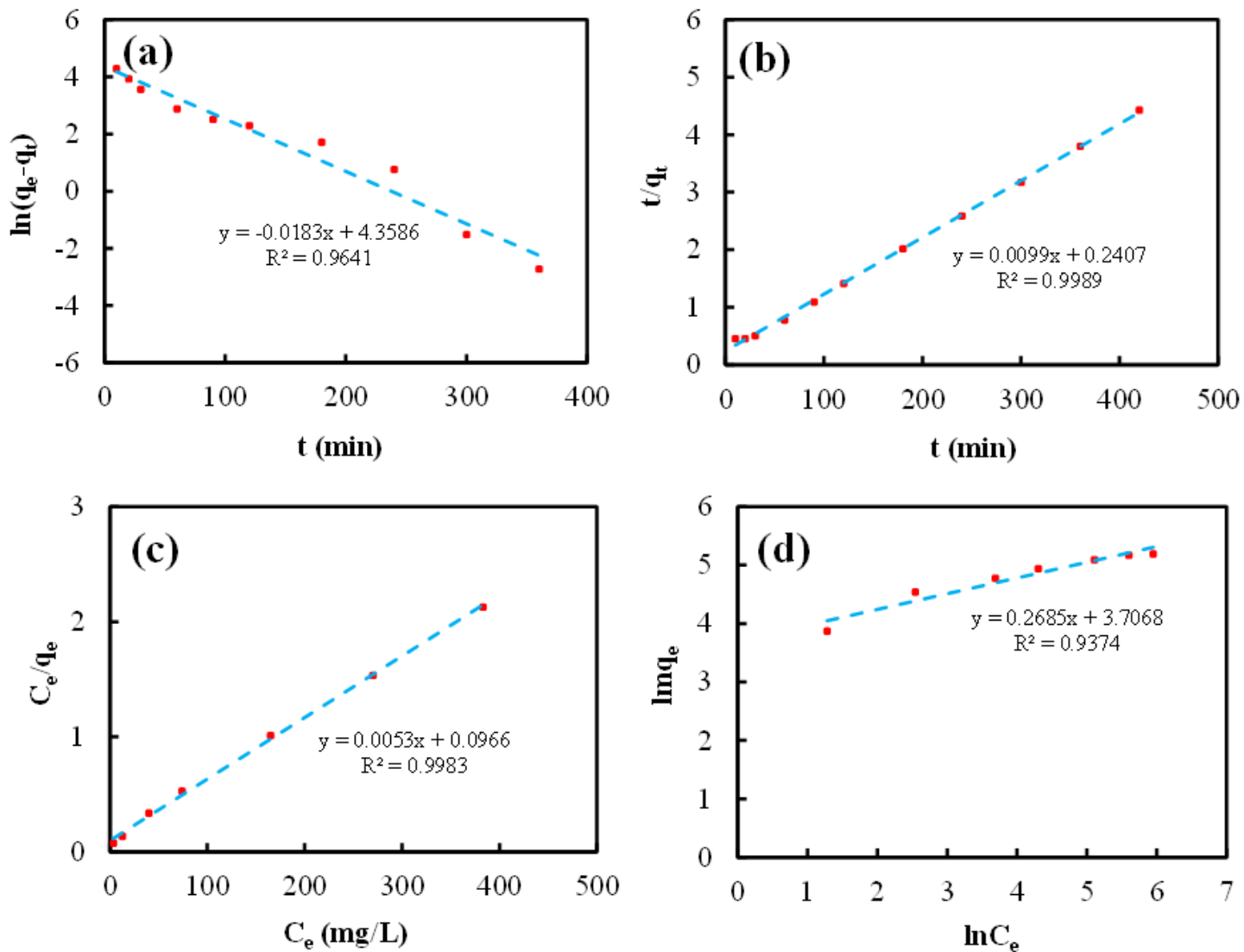
Figure 6

The adsorption kinetic and the adsorption isotherm for adsorption of Pb(II) ions in solution by PS-Fe3O4 composites (a: pseudo first-order kinetic model; b: pseudo second-order kinetic model; c: Langmuir isotherm model and d: Freundlich isotherm model)
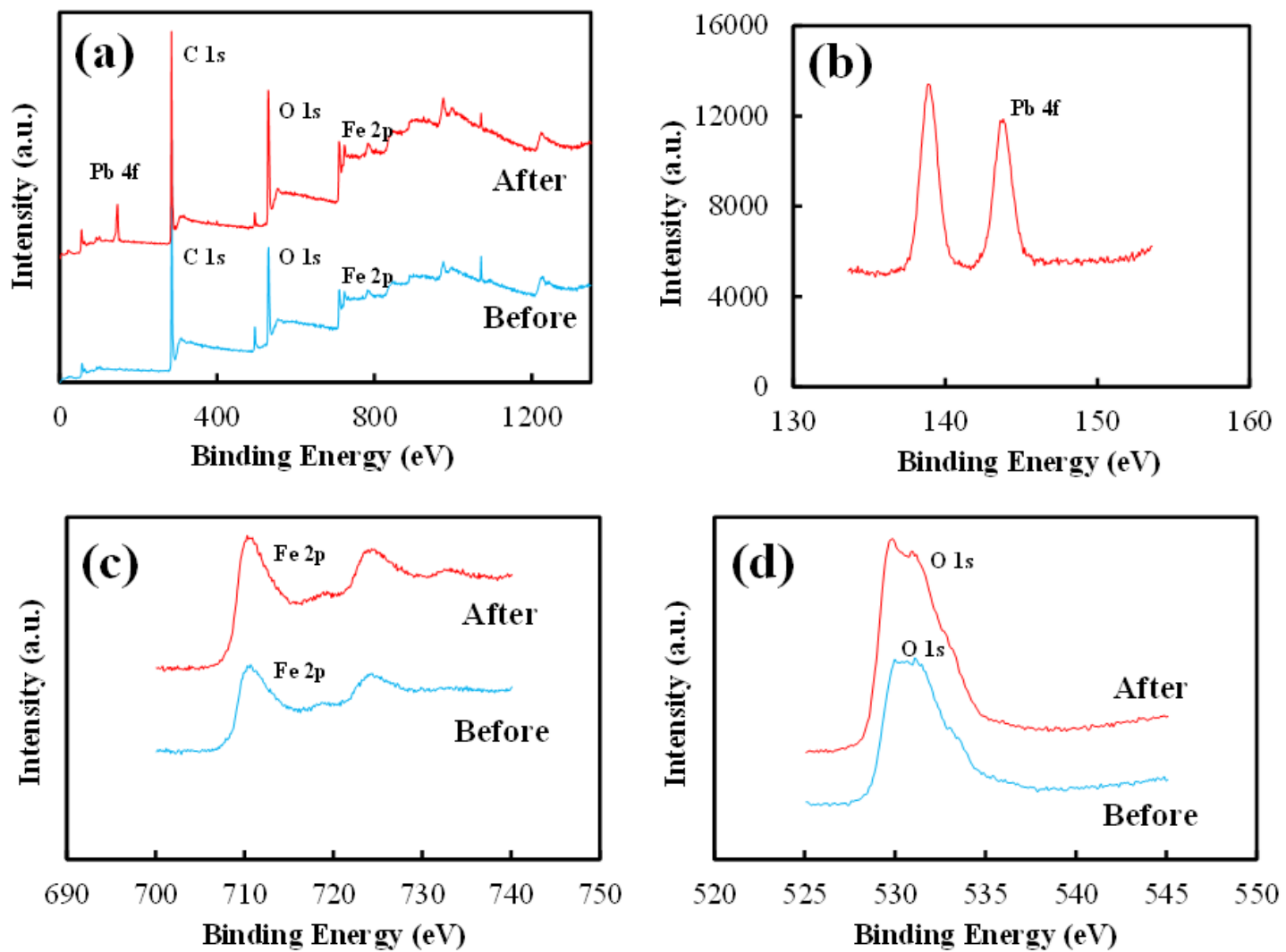
Figure 7

XSP spectra of PS-Fe3O4 composites before and after adsorption of Pb(II) ions (a: survey XPS; b: high resolved Pb 4f; c: high resolved Fe 2p; d: high resolved O 1s)
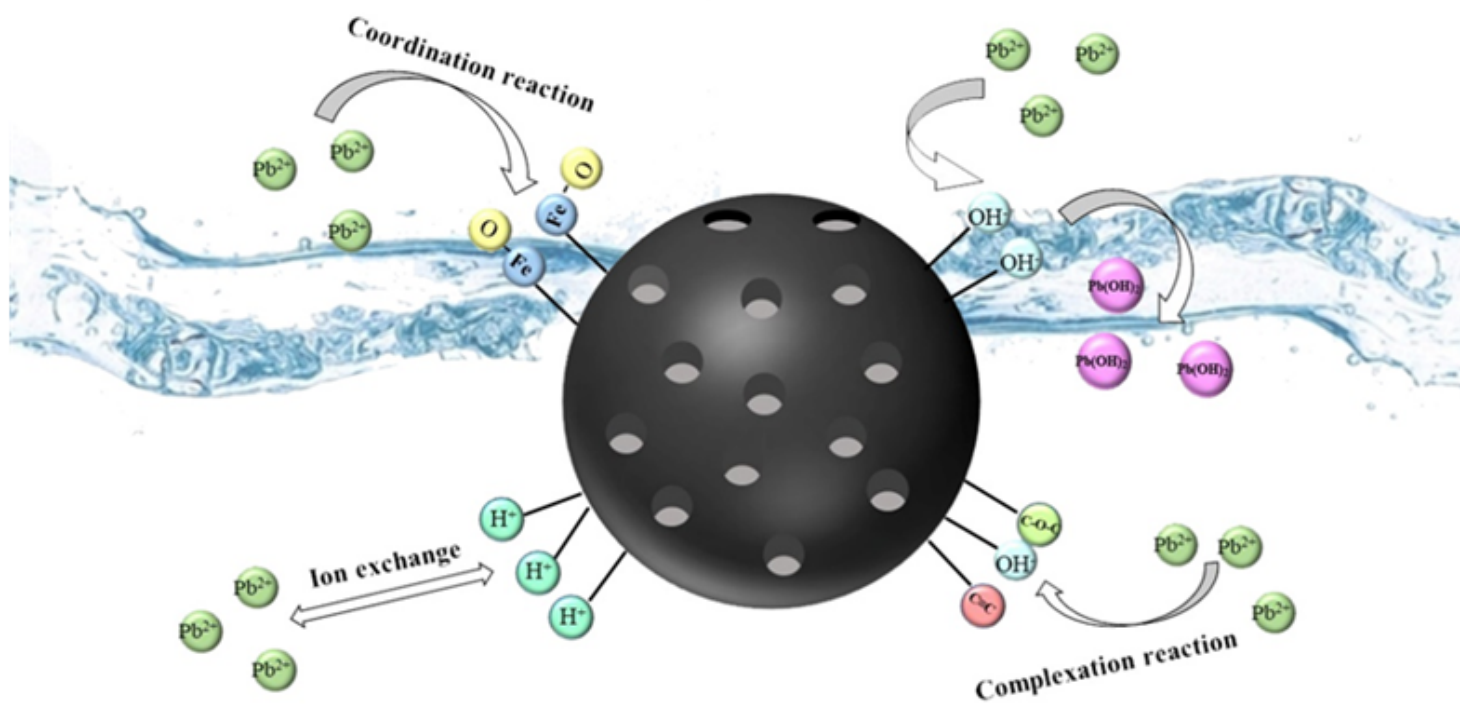
Figure 8

The possible mechanisms of Pb(II) ions removal in solution by PS-Fe3O4 composites
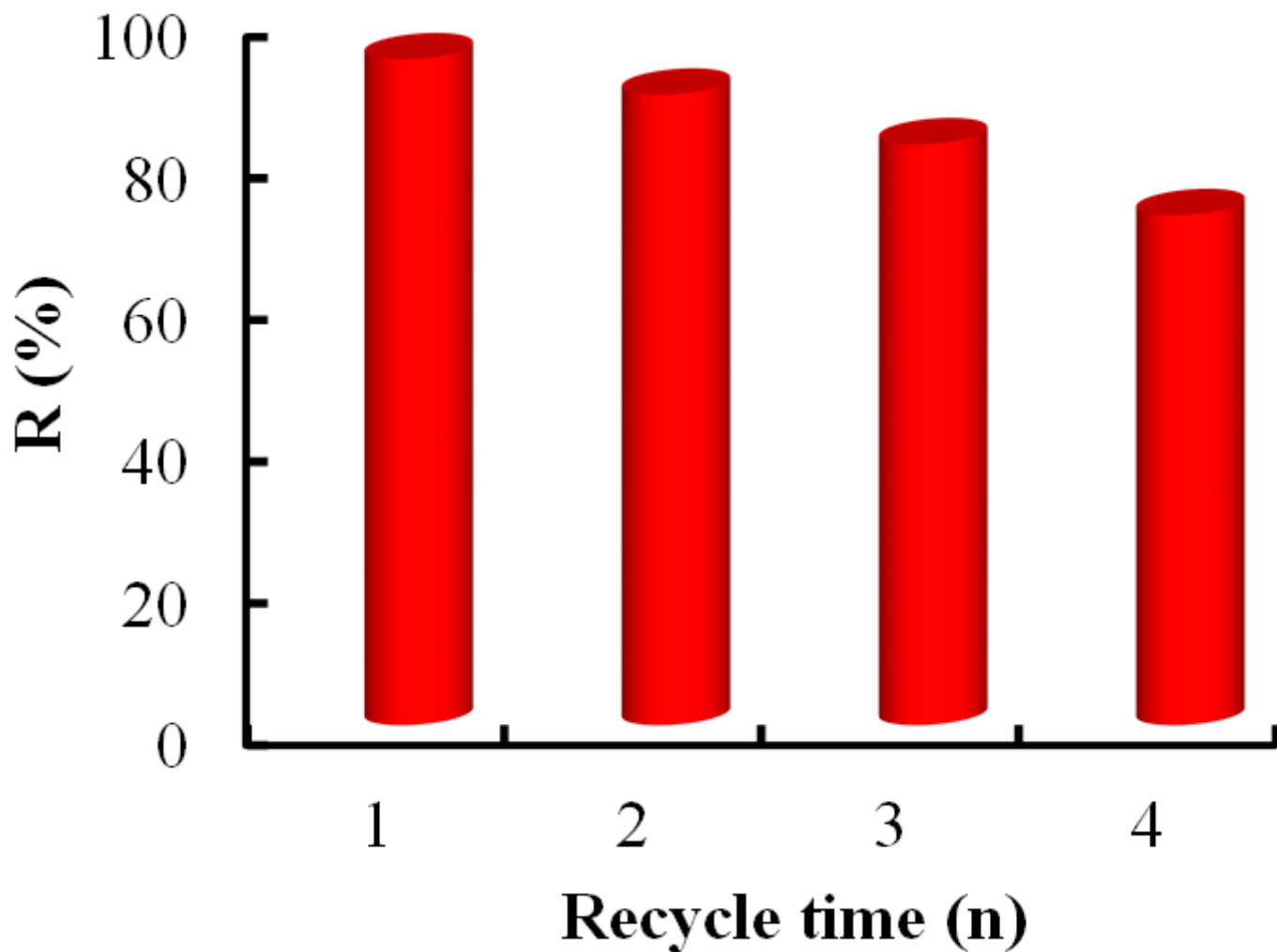
Figure 9

Influence of recycle time on adsorption rate of Pb(II) ions removal by PS-Fe3O4 composites

Supplementary Files

This is a list of supplementary files associated with this preprint. Click to download.

- Supplementmaterials.docx